NANO LETTERS

pubs.acs.org/NanoLett

Letter

Probing Chirality with Inelastic Electron-Light Scattering

Tyler R. Harvey,* Jan-Wilke Henke, Ofer Kfir, Hugo Lourenço-Martins, Armin Feist, F. Javier García de Abajo, and Claus Ropers*

Cite This: *Nano Lett.* 2020, 20, 4377−4383

Read Online

ACCESS | Metrics & More | Article Recommendations | Supporting Information

ABSTRACT: Circular dichroism spectroscopy is an essential technique for understanding molecular structure and magnetic materials; however, spatial resolution is limited by the wavelength of light, and sensitivity sufficient for single-molecule spectroscopy is challenging. We demonstrate that electrons can efficiently measure the interaction between circularly polarized light and chiral materials with deeply subwavelength resolution. By scanning a nanometer-sized focused electron beam across an optically excited chiral nanostructure and measuring the electron energy spectrum at each probe position, we produce a high-spatial-resolution map of near-field dichroism. This technique offers a nanoscale view of a fundamental symmetry and could be employed as "photon staining" to increase biomolecular material contrast in electron microscopy.

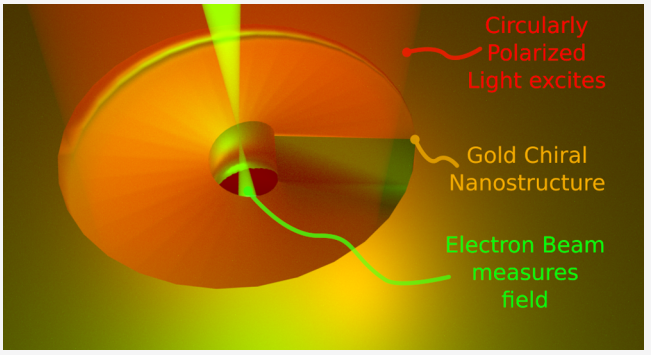

KEYWORDS: *circular dichroism, electron-light interaction, PINEM, nanophotonics, chirality, electron spectroscopy*

Chirality, defined as the absence of symmetry under spatial inversion, is central to a number of open scientific questions and technologically relevant materials, including the biochemistry of life,[1] the weak force and its potential connection to the chirality of biomolecules,[2] magnetic skyrmions,[3] and metamaterials.[4,5] Tools to probe chirality allow us insight into these phenomena; the first structural information about organic compounds came through studying the rotation of linearly polarized light in glucose solutions.[6] A related technique, circular dichroism (CD), is based on differences in absorption or scattering of circularly polarized light.

CD spectroscopy is widely employed to understand microscopic structure. X-ray magnetic circular dichroism[7,8] is a routine method for nanoscale magnetic domain imaging.[9] In biochemistry, circular dichroism spectroscopy serves as a molecular structural fingerprinting technique; the combination of local structural chirality and an optical transition necessary to produce a peak in a CD spectrum is more selective than just an optical transition.[10] Distinct kinds of molecular structural information are accessible through circular dichroism depending on the wavelength range. Secondary structure (e.g., α-helices and β-sheets, the small collections of hydrogen bonds that constitute segments of proteins) produces distinguishable far-UV CD spectra.[11] Near-UV CD spectra are sensitive to tertiary structure, the global arrangement of all of the segments.[12] Vibrational circular dichroism can retrieve structural information in conjunction with DFT calculations.[13]

These far-field circular dichroism techniques have some limitations. Because of the diffraction limit, spatial resolution is tied to the wavelength of light. The chiral contribution to molecular absorption is many orders of magnitude smaller than the nonchiral contribution; limited sensitivity necessitates the use of large ensembles of molecules.[10,14] One potential route toward higher sensitivity is to enhance the chiral part of optical absorption with spatially structured fields.[14−21] Another option is to measure near fields. Scanning near-field optical microscopy can be employed to measure near-field circular dichroism at surfaces, but resolution and bandwidth are limited by the tip and care must be taken to preserve polarization.[22,23] Photoemission electron microscopy can measure optical near fields with high spatial and temporal resolution[24−29] and illuminate spin-dependent plasmon dynamics;[30−32] the technique is also commonly used in conjunction with X-ray magnetic circular dichroism.[33,34] Cathodoluminescence polarimetry is another promising new approach to probe optical interactions with nanometer resolution and access to polarization.[35] Dichroism via exchange of electron orbital angular momentum and energy offers similar information without light.[36−39]

Received: March 13, 2020
Revised: April 28, 2020
Published: May 8, 2020

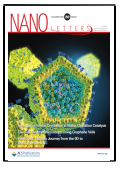

https://dx.doi.org/10.1021/acs.nanolett.0c01130
Nano Lett. 2020, 20, 4377−4383

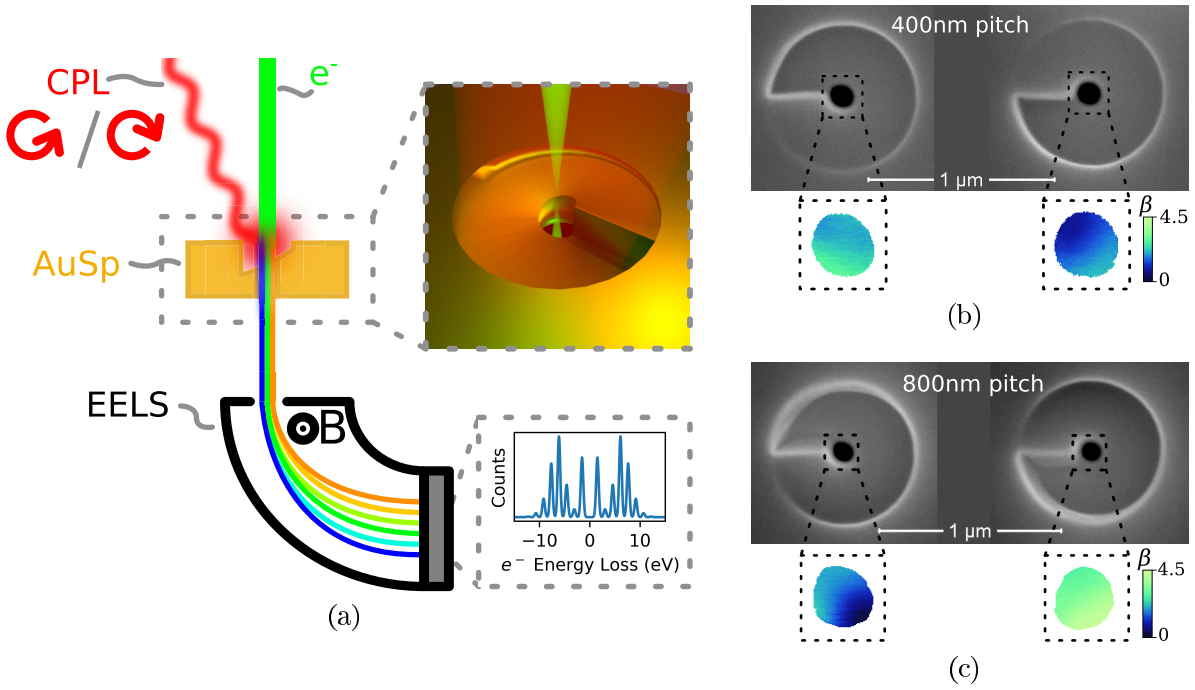

Figure 1. (a) Schematic of the experiment. The probe electron pulse (e^-, green) and circularly polarized optical pulse (CPL, red) are nearly colinearly incident on the specimen (AuSp, gold). Coupling to the optical field produces electron energy sidebands that are measured in an electron energy-loss spectrometer (EELS, black). Measurement of the associated coupling coefficient, $|\beta_\sigma(\mathbf{r}_\perp)|$, at each electron probe position produces a spatial map. (b) Scanning electron micrograph of the specimen measured in Figure 2, 400 nm pitch, 800 nm outer diameter spirals of opposite handedness milled into a 1 μm-thick gold slab with a 100 nm diameter hole. Insets depict PINEM maps with left-circularly polarized light, as shown in Figure 2c. (c) Scanning electron micrograph and inset PINEM maps of a different specimen with 800 nm pitch, showing a reversed relationship between handedness and coupling strength compared to (b). This difference highlights the three-dimensional structural information captured in these two-dimensional images.

Measurement of externally pumped optical near fields is possible in transmission electron microscopes. Although free-space absorption or emission of a photon by an electron is forbidden as it cannot conserve both energy and momentum, electrons in optical fields adjacent to or inside materials can exchange quantized momentum and energy with the field.[40,41] Barwick et al. employed this interaction to map optical near fields driven by laser illumination of the specimen; they called this technique photon-induced near-field electron microscopy (PINEM).[42] As near fields in an ultrafast transmission electron microsope can be sufficiently strong that the probability for an electron to lose or gain one or more units of photon energy is higher than the probability to exchange no energy,[43−45] PINEM is a highly sensitive probe of optical near fields and has been employed to image single-atom-high step edges,[46] proteins,[47] cells,[48] and nanoparticles.[49] While most applications of PINEM so far have relied on ultrashort electron and optical pulses to increase the strength of the optical field, the same interaction is possible with a continuous electron beam.[50,51] In this work, we demonstrate a near-field circular dichroism technique based on inelastic electron-light scattering. A unitless parameter β characterizes the local strength of the coupling between the near field and the electron beam,[43,44,52] where

$$\beta_\sigma(\mathbf{r}_\perp) = \frac{e}{\hbar\omega_{\mathrm{ph}}} \int \mathrm{d}z\, E_z(\mathbf{r}) \mathrm{e}^{-i\omega_{\mathrm{ph}} z/v_e} \tag{1}$$

depends on transverse electron beam position $\mathbf{r}_\perp$, electron velocity v_e, and the longitudinal component of the electric field in or near the material $E_z(\mathbf{r},\sigma,\omega_{\mathrm{ph}})$. This field depends on optical illumination helicity σ and photon energy $\hbar\omega_{\mathrm{ph}}$. The exchange of m quanta of energy with the optical field produces an electron energy distribution with a series of peaks at energies separated by $\hbar\omega_{\mathrm{ph}}$ with probabilities given by[43−45] $P_m = |J_m(2|\beta|)|^2$ (see the Supporting Information, page 4, for a more detailed description of the resulting spectra). A calculated example spectrum is shown in Figure 1a.

Because electron beams can be focused to subnanometer spots in modern electron microscopes, this interaction probes the optical response of materials with nanometer spatial resolution. Electron near-field circular dichroism (ENFCD) then can be defined as the normalized difference in β measured with left- and right-circularly polarized light:

$$\Delta(\mathbf{r}_\perp) = \frac{|\beta_{\mathrm{LCP}}| - |\beta_{\mathrm{RCP}}|}{|\beta_{\mathrm{LCP}}| + |\beta_{\mathrm{RCP}}|} \tag{2}$$

Spatial variations in Δ offer insight into the microscopic origins of chiral optical responses. Access to this information is not available at high spatial resolution through far-field circular dichroism, where the response is typically modeled with a small number of dipole transition moments.[53] This contrast mechanism can be employed for "photon staining" to boost contrast on biomolecular materials that only weakly scatter electrons.

We measured ENFCD on a prototypical chiral specimen that exemplifies this nondipolar spatial variation, as shown in Figure 1b. We prepared two nearly identical spirals of opposite handedness by FIB milling a 1 μm-thick gold slab. As the chirality in this specimen arises from geometry, we sought insight from optical field simulations. We numerically

https://dx.doi.org/10.1021/acs.nanolett.0c01130
Nano Lett. 2020, 20, 4377−4383

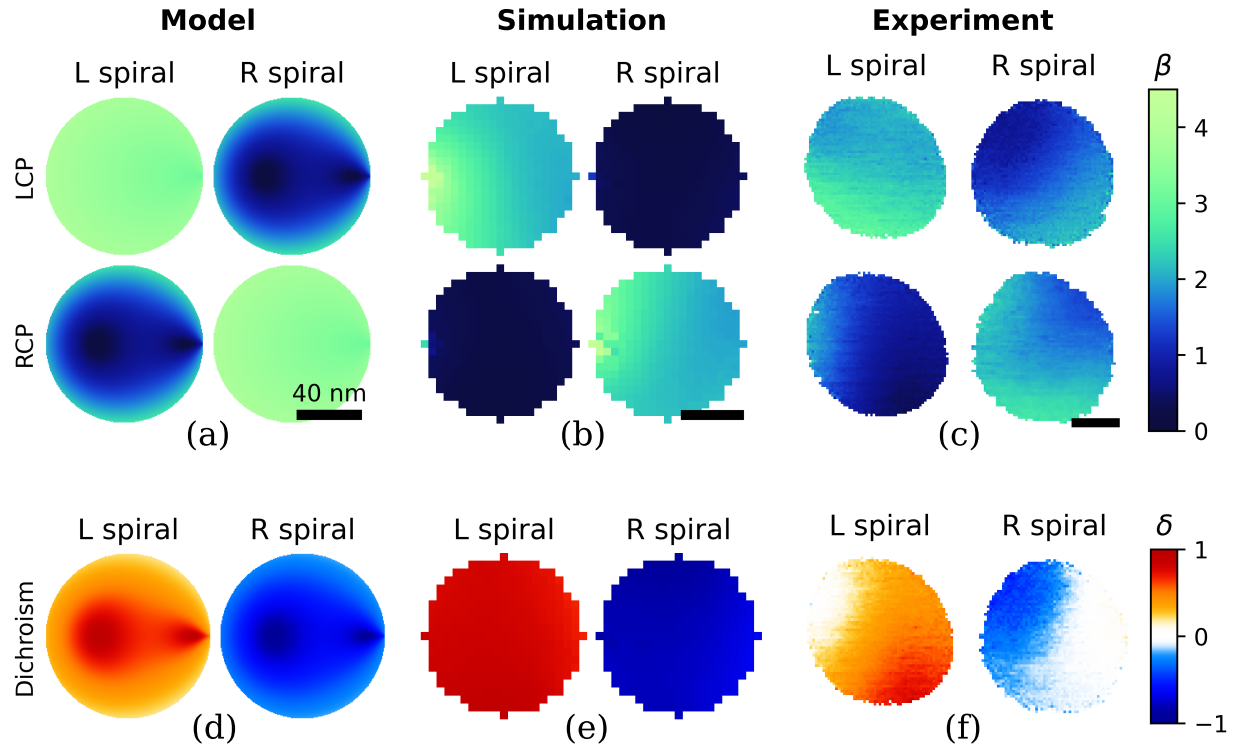

Figure 2. (a) 1D helix model, (b) finite-element simulated, and (c) experimental maps of the coupling coefficient $\beta_\sigma(\mathbf{r}_\perp)$ across the hole in the left-handed structure (left) and the right-handed structure (right) with left-circularly polarized (LCP, top) and right-circularly polarized (RCP, bottom) light. (d) Modeled, (e) simulated, and (f) experimental maps of the dichroism $\Delta(\mathbf{r}_\perp)$. The scale bar is 40 nm in all images.

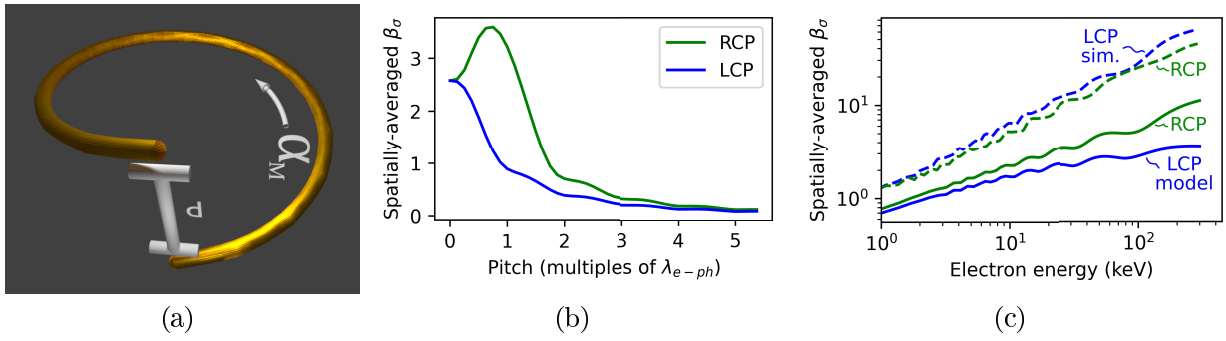

Figure 3. (a) Schematic of the model 1D helix with magnetic polarizability α_M along the helix axis and pitch d. (b) Calculated dependence of the hole-spatial-average coupling coefficients β_{LCP} (blue) and β_{RCP} (green) on the pitch of the model 1D helix with a diameter of 100 nm, optical wavelength of 800 nm, and electron energy of 200 keV. The minima occur at integer multiples of the coupling period $\lambda_{e\text{-}ph}$ = 554 nm. (c) Calculated electron energy dependence of the average coupling coefficients from the model 1D helix (solid lines) and from finite element simulations (dashed lines) with helix pitch and optical wavelength both at 800 nm. The same oscillatory behavior occurs as $\lambda_{e\text{-}ph}$ depends on energy, although it is only qualitatively similar behavior in the finite element simulation as there are likely other contributions to the response. Note that when the helix pitch matches the optical wavelength, the resonant coupling energy is infinity, so no maximum occurs here. Relative light intensities between model and simulations are chosen for visibility of lines.

calculated ENFCD in these structures based on frequency-domain finite element simulation of the optical fields with the COMSOL Multiphysics package. The simulations (Figure 2b) show that the spatial average of β inside the hole in the structure strongly depends on the optical helicity, and the relationship flips with the structure's handedness. In order to better understand the physical origins of spatial variations in ENFCD, we also developed a model for the optical response of the specimen, which we describe in more detail below and on Supporting Information page 14. The model (Figure 2a) also shows a helicity-dependent average β.

We performed measurements using the Göttingen JEOL 2100F ultrafast transmission electron microscope.[54] Circularly polarized 5 ps, 42 nJ optical pump pulses with an 800 nm central wavelength illuminated the specimen at nearly normal incidence with a 600 kHz repetition rate, as shown in Figure 1a. We raster-scanned 1 ps electron probe pulses focused to a spot size smaller than 10 nm over the hole in the spiral structures. An electron energy-loss spectrometer recorded an electron spectrum at each probe position, and we measured β from each spectrum by least-squares minimization with modeled spectra (see Supporting Information page 4 for a more detailed description of the β-measurement procedure).

https://dx.doi.org/10.1021/acs.nanolett.0c01130
Nano Lett. 2020, 20, 4377−4383

The resulting experimental maps of $\beta_\sigma(\mathbf{r}_\perp)$, shown in Figure 2c, agree with simulations regarding the relationship between structure and illumination handedness but show more spatial variation than both the model (Figure 2a) and simulations (Figure 2b). The larger spatial variation in the experimental maps likely arises due to additional contributions to the optical response from real features (e.g., smoother edges, finite slope of the spiral cut, and small optical coupling with other features in the surrounding region) that are not included in the simulations. These nanoscale spatial variations in ENFCD offer information about the three-dimensional structure and insight into the microscopic origins of chirality.

We considered two related descriptions of the spatial variations in ENFCD. First, for molecules or other specimens with a finite number of electronic transitions with limited coupling between them, it may be possible to match measured ENFCD maps with a model based on a sum of dipole transition moments. Following previous work,[55] we derive the equation for PINEM in this case in the Supporting Information (equation S26). Second, for specimens where collective excitations of many states contribute most to the optical response, we developed a model based on a simplified one-dimensional structure. At the 800 nm optical wavelength we used, gold can be treated as a good conductor with a skin depth much smaller than the size of the holes in the spirals we fabricated. We therefore represent these spirals as a 1D single-turn helix with a magnetic polarizability tangential to the edge of the helix, corresponding to a magnetic polarizability along the inner edge of the hole in the spiral. The simple helix model does not include additional features like the cut in the spiral, which we expect is responsible for the reversal of the sign of dichroism as a function of pitch (Figure 1c and Supporting Information Figures S1 and S2) that we see in simulation and experiment.

This model predicts an oscillatory response of the integrated coupling coefficient as a function of pitch d of the spiral for both circular polarizations within the hole, as shown in Figure 3b, with a coupling period corresponding to the momentum mismatch $\lambda_{e\text{-}ph} = 2\pi v_e/\omega_{ph}$. At $d = \lambda_{e\text{-}ph}$, the integrated relative dichroism is maximized. When the pitch is an integer multiple of $\lambda_{e\text{-}ph}$, the spatial symmetries of the coupling coefficient (Figure S6 in the Supporting Information) suggest that spin-to-orbital angular momentum conversion[30−32,56] determines the response: at a pitch $d = n\lambda_{e\text{-}ph}$, the coupling coefficient has $n + \sigma$ rotational symmetry, where σ is the helicity of the exciting light. The resonant dependence of the coupling coefficient on pitch as a function of $\lambda_{e\text{-}ph}$ suggests that we can boost the strength of dichroism, and therefore structural information obtained, by tuning either the electron kinetic energy or the optical wavelength. We have a recipe for maximization of the coupling coefficient and ENFCD for specimens with helical structural components such as α-helices or chiral plasmonic structures.[57−63] Specifically, this can be done by first setting the optical wavelength to known optical resonances and then tuning the electron energy to match $\lambda_{e\text{-}ph}$ to the helical pitch d of the structure. For example, for helical assemblies of semiconducting particles with a 390 nm pitch and a peak in optical circular dichroism at 690 nm,[64] resonant coupling occurs at 108 keV. This resonant coupling and high spatial resolution could be employed to image the assembly of helical nanostructures[58,60,61,65,66] *in situ*, or to visualize optical coupling between molecules and nanostructures for molecular sensing.[67,68] It may be possible to produce stronger dichroism using these two knobs than is possible in a linear optical technique where the light wavelength at which absorption occurs is far from the characteristic length scales associated with chirality. This tunable, resonant dichroism could also find application in dielectric laser acceleration[69−71] for helicity-controlled acceleration.

We have demonstrated a technique to measure circular dichroism in optical near fields with nanometer resolution. The spatially varying near-field dichroism we measure offers nanoscale detail not accessible through far-field optical circular dichroism. More information will be available with ENFCD spectroscopy, using a range of optical pump wavelengths to measure the full spatial and spectral response of a specimen. The available wavelength range is limited only by the laser source and optics used to illuminate the sample and can therefore be very broad. On the other hand, it may be possible to achieve single-molecule sensitivity over a limited wavelength range with the Purcell effect through coupling of molecular electronic states to the substrate or nanostructures. The local nature of our measurement means that coupling to an electric dipole is sufficient to enhance sensitivity.[72] As inelastic electron-light scattering is coherent, further sensitivity through interferometric measurement of the coupling coefficient is possible.[73−75] Temporal resolution is also available with ENFCD. The probe pulses we used in this work always arrived at the peak of the optical pump pulses, but temporal measurement of long-lived optical excitations in chiral materials is straightforward by varying probe−pulse arrival time. Chiral magnetization, polarization, or structural dynamics could be probed with ENFCD using a first optical pulse to pump the specimen and a second, weaker optical pulse overlapped with the delayed probe pulse. Access to nanoscale near-field circular dichroism spectra enables high-spatial-resolution characterization of three-dimensional structure with straightforward extension to temporal resolution and possibilities for single-molecule sensitivity.

■ ASSOCIATED CONTENT

Supporting Information

The Supporting Information is available free of charge at https://pubs.acs.org/doi/10.1021/acs.nanolett.0c01130.

Additional measurements of electron near-field circular dichroism and linear dichroism measurements; details on the polarization calibration; procedure used in finite-element simulations; coupling coefficient uncertainty calculation; discussion of experimental sources of error; coupling coefficient calculation for inelastic electron−photon interactions with oscillating electric and magnetic dipoles; and model of the specimen with a 1D polarizability (PDF)

■ AUTHOR INFORMATION

Corresponding Authors

Tyler R. Harvey − *Georg-August-Universität Göttingen, D-37077 Göttingen, Germany*; orcid.org/0000-0002-5368-136X; Email: harvey@ph4.physik.uni-goettingen.de

Claus Ropers − *Georg-August-Universität Göttingen, D-37077 Göttingen, Germany*; Email: claus.ropers@uni-goettingen.de

Authors

Jan-Wilke Henke − *Georg-August-Universität Göttingen, D-37077 Göttingen, Germany*

https://dx.doi.org/10.1021/acs.nanolett.0c01130
Nano Lett. 2020, 20, 4377−4383

Ofer Kfir − *Georg-August-Universität Göttingen, D-37077 Göttingen, Germany;* orcid.org/0000-0003-1253-9372
Hugo Lourenço-Martins − *Georg-August-Universität Göttingen, D-37077 Göttingen, Germany*
Armin Feist − *Georg-August-Universität Göttingen, D-37077 Göttingen, Germany;* orcid.org/0000-0003-1434-8895
F. Javier García de Abajo − *ICFO-Institut de Ciencies Fotoniques, The Barcelona Institute of Science and Technology, 08860 Castelldefels, Barcelona, Spain; ICREA-Institució Catalana de Recerca i Estudis Avançats, 08010 Barcelona, Spain;* orcid.org/0000-0002-4970-4565

Complete contact information is available at: https://pubs.acs.org/10.1021/acs.nanolett.0c01130

Notes

The authors declare no competing financial interest.

■ ACKNOWLEDGMENTS

We appreciate the work the Göttingen UTEM team has put into developing the microscope. We acknowledge helpful discussions with Katharina Priebe, Murat Sivis, and Benjamin McMorran. We acknowledge financial support by the Deutsche Forschungsgemeinschaft through SPP 1840 QUTIF and the Leibniz program. O.K. gratefully acknowledges funding from the European Union's Horizon 2020 research and innovation programme under the Marie Skłodowska-Curie grant agreement no.752533. F.J.G.A. acknowledges support from ERC (advanced grant 789104-eNANO) and the Spanish MINECO (MAT2017-88492-R and SEV2015-0522). T.R.H. acknowledges the support of a postdoctoral fellowship from the Alexander von Humboldt Foundation and its sponsor, the German Federal Ministry for Education and Research.

■ REFERENCES

(1) Evans, A. C.; Meinert, C.; Giri, C.; Goesmann, F.; Meierhenrich, U. J. Chirality, photochemistry and the detection of amino acids in interstellar ice analogues and comets. *Chem. Soc. Rev.* **2012**, *41*, 5447−5458.
(2) Dreiling, J. M.; Gay, T. J. Chirally Sensitive Electron-Induced Molecular Breakup and the Vester-Ulbricht Hypothesis. *Phys. Rev. Lett.* **2014**, *113*, 118103.
(3) Yu, X. Z.; Onose, Y.; Kanazawa, N.; Park, J. H.; Han, J. H.; Matsui, Y.; Nagaosa, N.; Tokura, Y. Real-space observation of a two-dimensional skyrmion crystal. *Nature* **2010**, *465*, 901−904.
(4) Tretyakov, S. A.; Sihvola, A. H.; Sochava, A. A.; Simovski, C. R. Magnetoelectric Interactions in Bi-Anisotropic Media. *Journal of Electromagnetic Waves and Applications* **1998**, *12*, 481−497.
(5) Zhang, S.; Park, Y.-S.; Li, J.; Lu, X.; Zhang, W.; Zhang, X. Negative Refractive Index in Chiral Metamaterials. *Phys. Rev. Lett.* **2009**, *102*, No. 023901.
(6) Drayer, D. E. The Early History of Stereochemistry: From the Discovery of Molecular Asymmetry and the First Resolution of a Racemate by Pasteur to the Asymmetrical Chiral Carbon of Van't Hoff and Le Bel*. *Clinical Research and Regulatory Affairs* **2001**, *18*, 181−203.
(7) Thole, B. T.; Carra, P.; Sette, F.; van der Laan, G. X-ray circular dichroism as a probe of orbital magnetization. *Phys. Rev. Lett.* **1992**, *68*, 1943−1946.
(8) Stöhr, J. X-ray magnetic circular dichroism spectroscopy of transition metal thin films. *J. Electron Spectrosc. Relat. Phenom.* **1995**, *75*, 253−272.
(9) Stöhr, J.; Padmore, H. A.; Anders, S.; Stammler, T.; Scheinfein, M. R. Principles of X-Ray Magnetic Dichroism Spectromicroscopy. *Surf. Rev. Lett.* **1998**, *05*, 1297−1308.
(10) Purdie, N.; Swallows, K. A. Analytical applications of polarimetry, optical rotatory dispersion, and circular dichroism. *Anal. Chem.* **1989**, *61*, 77A−89A.
(11) Johnson, W. C. Protein secondary structure and circular dichroism: A practical guide. *Proteins: Struct., Funct., Genet.* **1990**, *7*, 205−214.
(12) Li, C. H.; Nguyen, X.; Narhi, L.; Chemmalil, L.; Towers, E.; Muzammil, S.; Gabrielson, J.; Jiang, Y. Applications of circular dichroism (CD) for structural analysis of proteins: qualification of near- and far-UV CD for protein higher order structural analysis. *J. Pharm. Sci.* **2011**, *100*, 4642−4654.
(13) Stephens, P. J.; Devlin, F. J.; Pan, J.-J. The determination of the absolute configurations of chiral molecules using vibrational circular dichroism (VCD) spectroscopy. *Chirality* **2008**, *20*, 643−663.
(14) Rhee, H.; Choi, J. S.; Starling, D. J.; Howell, J. C.; Cho, M. Amplifications in chiroptical spectroscopy, optical enantioselectivity, and weak value measurement. *Chemical Science* **2013**, *4*, 4107−4114.
(15) Tang, Y.; Cohen, A. E. Optical Chirality and Its Interaction with Matter. *Phys. Rev. Lett.* **2010**, *104*, 163901.
(16) Bliokh, K. Y.; Nori, F. Characterizing optical chirality. *Phys. Rev. A: At., Mol., Opt. Phys.* **2011**, *83*, No. 021803.
(17) Choi, J. S.; Cho, M. Limitations of a superchiral field. *Phys. Rev. A: At., Mol., Opt. Phys.* **2012**, *86*, No. 063834.
(18) Coles, M. M.; Andrews, D. L. Chirality and angular momentum in optical radiation. *Phys. Rev. A: At., Mol., Opt. Phys.* **2012**, *85*, No. 063810.
(19) Barr, L. E.; Horsley, S. A. R.; Hooper, I. R.; Eager, J. K.; Gallagher, C. P.; Hornett, S. M.; Hibbins, A. P.; Hendry, E. Investigating the nature of chiral near-field interactions. *Phys. Rev. B: Condens. Matter Mater. Phys.* **2018**, *97*, 155418.
(20) Poulikakos, L. V.; Thureja, P.; Stollmann, A.; De Leo, E.; Norris, D. J. Chiral Light Design and Detection Inspired by Optical Antenna Theory. *Nano Lett.* **2018**, *18*, 4633−4640.
(21) Poulikakos, L. V.; Dionne, J. A.; García-Etxarri, A. Optical Helicity and Optical Chirality in Free Space and in the Presence of Matter. *Symmetry* **2019**, *11*, 1113.
(22) Narushima, T.; Okamoto, H. Circular dichroism nano-imaging of two-dimensional chiral metal nanostructures. *Phys. Chem. Chem. Phys.* **2013**, *15*, 13805−13809.
(23) Schnell, M.; Sarriugarte, P.; Neuman, T.; Khanikaev, A. B.; Shvets, G.; Aizpurua, J.; Hillenbrand, R. Real-Space Mapping of the Chiral Near-Field Distributions in Spiral Antennas and Planar Metasurfaces. *Nano Lett.* **2016**, *16*, 663−670.
(24) Kubo, A.; Pontius, N.; Petek, H. Femtosecond Microscopy of Surface Plasmon Polariton Wave Packet Evolution at the Silver/Vacuum Interface. *Nano Lett.* **2007**, *7*, 470−475.
(25) Kahl, P.; Wall, S.; Witt, C.; Schneider, C.; Bayer, D.; Fischer, A.; Melchior, P.; Horn-von Hoegen, M.; Aeschlimann, M.; Meyer zu Heringdorf, F.-J. Normal-Incidence Photoemission Electron Microscopy (NI-PEEM) for Imaging Surface Plasmon Polaritons. *Plasmonics* **2014**, *9*, 1401−1407.
(26) Gong, Y.; Joly, A. G.; Hu, D.; El-Khoury, P. Z.; Hess, W. P. Ultrafast Imaging of Surface Plasmons Propagating on a Gold Surface. *Nano Lett.* **2015**, *15*, 3472−3478.
(27) El-Khoury, P. Z.; Abellan, P.; Gong, Y.; Hage, F. S.; Cottom, J.; Joly, A. G.; Brydson, R.; Ramasse, Q. M.; Hess, W. P. Visualizing surface plasmons with photons, photoelectrons, and electrons. *Analyst* **2016**, *141*, 3562−3572.
(28) Dąbrowski, M.; Dai, Y.; Petek, H. Ultrafast Microscopy: Imaging Light with Photoelectrons on the Nano−Femto Scale. *J. Phys. Chem. Lett.* **2017**, *8*, 4446−4455.
(29) Frank, B.; Kahl, P.; Podbiel, D.; Spektor, G.; Orenstein, M.; Fu, L.; Weiss, T.; Horn-von Hoegen, M.; Davis, T. J.; Meyer zu Heringdorf, F.-J.; Giessen, H. Short-range surface plasmonics: Localized electron emission dynamics from a 60-nm spot on an atomically flat single-crystalline gold surface. *Science Advances* **2017**, *3*, No. e1700721.
(30) Spektor, G.; Kilbane, D.; Mahro, A. K.; Frank, B.; Ristok, S.; Gal, L.; Kahl, P.; Podbiel, D.; Mathias, S.; Giessen, H.; Meyer zu

Heringdorf, F.-J.; Orenstein, M.; Aeschlimann, M. Revealing the subfemtosecond dynamics of orbital angular momentum in nanoplasmonic vortices. *Science* **2017**, *355*, 1187−1191.
(31) Dai, Y.; Dąbrowski, M.; Apkarian, V. A.; Petek, H. Ultrafast Microscopy of Spin-Momentum-Locked Surface Plasmon Polaritons. *ACS Nano* **2018**, *12*, 6588−6596.
(32) Spektor, G.; Kilbane, D.; Mahro, A. K.; Hartelt, M.; Prinz, E.; Aeschlimann, M.; Orenstein, M. Mixing the Light Spin with Plasmon Orbit by Nonlinear Light-Matter Interaction in Gold. *Phys. Rev. X* **2019**, *9*, No. 021031.
(33) Vogel, J.; Kuch, W.; Bonfim, M.; Camarero, J.; Pennec, Y.; Offi, F.; Fukumoto, K.; Kirschner, J.; Fontaine, A.; Pizzini, S. Time-resolved magnetic domain imaging by x-ray photoemission electron microscopy. *Appl. Phys. Lett.* **2003**, *82*, 2299−2301.
(34) Cheng, X. M.; Keavney, D. J. Studies of nanomagnetism using synchrotron-based x-ray photoemission electron microscopy (X-PEEM). *Rep. Prog. Phys.* **2012**, *75*, No. 026501.
(35) Osorio, C. I.; Coenen, T.; Brenny, B. J. M.; Polman, A.; Koenderink, A. F. Angle-Resolved Cathodoluminescence Imaging Polarimetry. *ACS Photonics* **2016**, *3*, 147−154.
(36) Asenjo-Garcia, A.; García de Abajo, F. J. Dichroism in the Interaction between Vortex Electron Beams, Plasmons, and Molecules. *Phys. Rev. Lett.* **2014**, *113*, No. 066102.
(37) Harvey, T. R.; Pierce, J. S.; Chess, J. J.; McMorran, B. J. Demonstration of electron helical dichroism as a local probe of chirality. *arXiv* (Condensed Matter, Materials Science), July 5, 2015, 1507.01810. https://arxiv.org/abs/1507.01810 (accessed 2020).
(38) Guzzinati, G.; Béché, A.; Lourenço-Martins, H.; Martin, J.; Kociak, M.; Verbeeck, J. Probing the symmetry of the potential of localized surface plasmon resonances with phase-shaped electron beams. *Nat. Commun.* **2017**, *8*, 1−8.
(39) Zanfrognini, M.; Rotunno, E.; Frabboni, S.; Sit, A.; Karimi, E.; Hohenester, U.; Grillo, V. Orbital Angular Momentum and Energy Loss Characterization of Plasmonic Excitations in Metallic Nanostructures in TEM. *ACS Photonics* **2019**, *6*, 620−627.
(40) Saathoff, G.; Miaja-Avila, L.; Aeschlimann, M.; Murnane, M. M.; Kapteyn, H. C. Laser-assisted photoemission from surfaces. *Phys. Rev. A: At., Mol., Opt. Phys.* **2008**, *77*, No. 022903.
(41) García de Abajo, F. J.; Kociak, M. Electron energy-gain spectroscopy. *New J. Phys.* **2008**, *10*, No. 073035.
(42) Barwick, B.; Flannigan, D. J.; Zewail, A. H. Photon-induced near-field electron microscopy. *Nature* **2009**, *462*, 902−906.
(43) Park, S. T.; Lin, M.; Zewail, A. H. Photon-induced near-field electron microscopy (PINEM): theoretical and experimental. *New J. Phys.* **2010**, *12*, 123028.
(44) García de Abajo, F. J.; Asenjo-Garcia, A.; Kociak, M. Multiphoton Absorption and Emission by Interaction of Swift Electrons with Evanescent Light Fields. *Nano Lett.* **2010**, *10*, 1859−1863.
(45) Feist, A.; Echternkamp, K. E.; Schauss, J.; Yalunin, S. V.; Schäfer, S.; Ropers, C. Quantum coherent optical phase modulation in an ultrafast transmission electron microscope. *Nature* **2015**, *521*, 200−203.
(46) Park, S. T.; Yurtsever, A.; Baskin, J. S.; Zewail, A. H. Graphene-layered steps and their fields visualized by 4D electron microscopy. *Proc. Natl. Acad. Sci. U. S. A.* **2013**, *110*, 9277−9282.
(47) Flannigan, D. J.; Barwick, B.; Zewail, A. H. Biological imaging with 4D ultrafast electron microscopy. *Proc. Natl. Acad. Sci. U. S. A.* **2010**, *107*, 9933−9937.
(48) Kaplan, M.; Yoo, B.-K.; Tang, J.; Karam, T. E.; Liao, B.; Majumdar, D.; Baltimore, D.; Jensen, G. J.; Zewail, A. H. Photon-Induced Near-Field Electron Microscopy of Eukaryotic Cells. *Angew. Chem., Int. Ed.* **2017**, *56*, 11498−11501.
(49) Yurtsever, A.; Zewail, A. H. Direct Visualization of Near-Fields in Nanoplasmonics and Nanophotonics. *Nano Lett.* **2012**, *12*, 3334−3338.
(50) Das, P.; Blazit, J. D.; Tencé, M.; Zagonel, L. F.; Auad, Y.; Lee, Y. H.; Ling, X. Y.; Losquin, A.; Colliex, C.; Stéphan, O.; García de Abajo, F. J.; Kociak, M. Stimulated electron energy loss and gain in an electron microscope without a pulsed electron gun. *Ultramicroscopy* **2019**, *203*, 44−51.
(51) Liu, C.; Wu, Y.; Hu, Z.; Busche, J. A.; Beutler, E. K.; Montoni, N. P.; Moore, T. M.; Magel, G. A.; Camden, J. P.; Masiello, D. J.; Duscher, G.; Rack, P. D. Continuous Wave Resonant Photon Stimulated Electron Energy-Gain and Electron Energy-Loss Spectroscopy of Individual Plasmonic Nanoparticles. *ACS Photonics* **2019**, *6*, 2499−2508.
(52) García de Abajo, F. J.; Barwick, B.; Carbone, F. Electron diffraction by plasmon waves. *Phys. Rev. B: Condens. Matter Mater. Phys.* **2016**, *94*, No. 041404.
(53) Power, E. A.; Thirunamachandran, T. Circular dichroism: A general theory based on quantum electrodynamics. *J. Chem. Phys.* **1974**, *60*, 3695−3701.
(54) Feist, A.; Bach, N.; Rubiano da Silva, N.; Danz, T.; Möller, M.; Priebe, K. E.; Domröse, T.; Gatzmann, J. G.; Rost, S.; Schauss, J.; Strauch, S.; Bormann, R.; Sivis, M.; Schäfer, S.; Ropers, C. Ultrafast Transmission Electron Microscopy Using a Laser-Driven Field Emitter: Femtosecond Resolution with a High Coherence Electron Beam. *Ultramicroscopy* **2017**, *176*, 63−73.
(55) Di Giulio, V.; Kociak, M.; García de Abajo, F. J. Probing quantum optical excitations with fast electrons. *Optica* **2019**, *6*, 1524−1534.
(56) Vanacore, G. M.; Berruto, G.; Madan, I.; Pomarico, E.; Biagioni, P.; Lamb, R. J.; McGrouther, D.; Reinhardt, O.; Kaminer, I.; Barwick, B.; Larocque, H.; Grillo, V.; Karimi, E.; García de Abajo, F. J.; Carbone, F. Ultrafast generation and control of an electron vortex beam via chiral plasmonic near fields. *Nat. Mater.* **2019**, *18*, 573−579.
(57) Fan, Z.; Govorov, A. O. Plasmonic Circular Dichroism of Chiral Metal Nanoparticle Assemblies. *Nano Lett.* **2010**, *10*, 2580−2587.
(58) Kuzyk, A.; Schreiber, R.; Fan, Z.; Pardatscher, G.; Roller, E.-M.; Högele, A.; Simmel, F. C.; Govorov, A. O.; Liedl, T. DNA-based self-assembly of chiral plasmonic nanostructures with tailored optical response. *Nature* **2012**, *483*, 311−314.
(59) Hentschel, M.; Schäferling, M.; Weiss, T.; Liu, N.; Giessen, H. Three-Dimensional Chiral Plasmonic Oligomers. *Nano Lett.* **2012**, *12*, 2542−2547.
(60) Shen, X.; Asenjo-Garcia, A.; Liu, Q.; Jiang, Q.; García de Abajo, F. J.; Liu, N.; Ding, B. Three-Dimensional Plasmonic Chiral Tetramers Assembled by DNA Origami. *Nano Lett.* **2013**, *13*, 2128−2133.
(61) Song, C.; Blaber, M. G.; Zhao, G.; Zhang, P.; Fry, H. C.; Schatz, G. C.; Rosi, N. L. Tailorable Plasmonic Circular Dichroism Properties of Helical Nanoparticle Superstructures. *Nano Lett.* **2013**, *13*, 3256−3261.
(62) Hentschel, M.; Schäferling, M.; Duan, X.; Giessen, H.; Liu, N. Chiral plasmonics. *Science Advances* **2017**, *3*, No. e1602735.
(63) Saito, K.; Tatsuma, T. Chiral Plasmonic Nanostructures Fabricated by Circularly Polarized Light. *Nano Lett.* **2018**, *18*, 3209−3212.
(64) Yan, J.; Feng, W.; Kim, J.-Y.; Lu, J.; Kumar, P.; Mu, Z.; Wu, X.; Mao, X.; Kotov, N. A. Self-Assembly of Chiral Nanoparticles into Semiconductor Helices with Tunable near-Infrared Optical Activity. *Chem. Mater.* **2020**, *32*, 476−488.
(65) Srivastava, S.; Santos, A.; Critchley, K.; Kim, K.-S.; Podsiadlo, P.; Sun, K.; Lee, J.; Xu, C.; Lilly, G. D.; Glotzer, S. C.; Kotov, N. A. Light-Controlled Self-Assembly of Semiconductor Nanoparticles into Twisted Ribbons. *Science* **2010**, *327*, 1355−1359.
(66) Yan, W.; Xu, L.; Xu, C.; Ma, W.; Kuang, H.; Wang, L.; Kotov, N. A. Self-Assembly of Chiral Nanoparticle Pyramids with Strong R/S Optical Activity. *J. Am. Chem. Soc.* **2012**, *134*, 15114−15121.
(67) James, T. D.; Samankumara Sandanayake, K. R. A.; Shinkai, S. Chiral discrimination of monosaccharides using a fluorescent molecular sensor. *Nature* **1995**, *374*, 345−347.
(68) García-Guirado, J.; Svedendahl, M.; Puigdollers, J.; Quidant, R. Enantiomer-Selective Molecular Sensing Using Racemic Nanoplasmonic Arrays. *Nano Lett.* **2018**, *18*, 6279−6285.

https://dx.doi.org/10.1021/acs.nanolett.0c01130
Nano Lett. 2020, 20, 4377−4383

(69) Mizuno, K.; Pae, J.; Nozokido, T.; Furuya, K. Experimental evidence of the inverse Smith−Purcell effect. *Nature* **1987**, *328*, 45−47.
(70) Breuer, J.; Hommelhoff, P. Laser-Based Acceleration of Nonrelativistic Electrons at a Dielectric Structure. *Phys. Rev. Lett.* **2013**, *111*, 134803.
(71) Peralta, E. A.; Soong, K.; England, R. J.; Colby, E. R.; Wu, Z.; Montazeri, B.; McGuinness, C.; McNeur, J.; Leedle, K. J.; Walz, D.; Sozer, E. B.; Cowan, B.; Schwartz, B.; Travish, G.; Byer, R. L. Demonstration of electron acceleration in a laser-driven dielectric microstructure. *Nature* **2013**, *503*, 91−94.
(72) García-Etxarri, A.; Dionne, J. A. Surface-enhanced circular dichroism spectroscopy mediated by nonchiral nanoantennas. *Phys. Rev. B: Condens. Matter Mater. Phys.* **2013**, *87*, 235409.
(73) Echternkamp, K. E.; Feist, A.; Schäfer, S.; Ropers, C. Ramsey-type phase control of free-electron beams. *Nat. Phys.* **2016**, *12*, 1000−1004.
(74) Priebe, K. E.; Rathje, C.; Yalunin, S. V.; Hohage, T.; Feist, A.; Schäfer, S.; Ropers, C. Attosecond electron pulse trains and quantum state reconstruction in ultrafast transmission electron microscopy. *Nat. Photonics* **2017**, *11*, 793−797.
(75) Madan, I.; Vanacore, G. M.; Pomarico, E.; Berruto, G.; Lamb, R. J.; McGrouther, D.; Lummen, T. T. A.; Latychevskaia, T.; García de Abajo, F. J.; Carbone, F. Holographic imaging of electromagnetic fields via electron-light quantum interference. *Science Advances* **2019**, *5*, No. eaav8358.

https://dx.doi.org/10.1021/acs.nanolett.0c01130
Nano Lett. 2020, 20, 4377−4383